Energy Flux and Generation of Diurnal Shelf Waves along Vancouver Island

WILLIAM R. CRAWFORD

Institute of Ocean Sciences, Sidney, B.C., V8L 4B2, Canada

(Manuscript received 8 September 1983, in final form 5 June 1984)

ABSTRACT

Recent observations along the west coast of Vancouver Island reveal strong diurnal-period currents due to a tidally driven continental shelf wave superimposed upon a Kelvin wave. The energy flux of this system is investigated here. It is shown that both the Kelvin wave and the first-mode continental shelf wave transport energy toward the northwest in the direction of phase propagation, but when the two waves are superimposed the combined energy flux vectors form meanders and gyres over the continental shelf; the pattern repeats in the alongshore direction every wavelength of the shelf wave. Near Southern Vancouver Island these waves combine to form a gyre in which the nearshore side carries energy to the southeast toward Juan de Fuca Strait. Kinetic energy flows up-Strait until it is dissipated in narrow tidal channels.

The total alongshore energy flux in the shelf wave alone can be determined from a fit of a model baroclinic shelf wave to current meter observations along Vancouver Island. Energy flux in the K_1-period shelf wave decreases as the wave propagates away from Juan de Fuca Strait, probably because of wave dispersion rather than friction. The decrease in energy flux together with the convergence toward Juan de Fuca Strait of flux vectors of the combined waves suggests the shelf wave originates at the entrance to Juan de Fuca Strait.

1. Introduction

A unique feature of the continental shelf currents along the west coast of North America is the abrupt increase in diurnal-period currents north of Juan de Fuca Strait. Previous papers describe the nature of these currents, showing how they behave as northward propagating continental shelf waves (Crawford and Thomson, 1982; hereafter CT82) and that their behavior along the regular bottom topography at mid-Vancouver Island agrees well with the predicted behavior of baroclinic shelf waves (Crawford and Thomson, 1984; hereafter CT84). The origin of these waves has not been conclusively determined. Thomson and Crawford (1982) show that tidal currents due to large-scale (10^4 km) Kelvin waves could excite continental shelf waves of shorter wavelength (10^2 to 10^3 km) along a shelf but that the rate of energy transfer is low. We note (CT82) that the abrupt beginning of the waves near Juan de Fuca Strait and the continuity of phase of the currents in the Strait and the adjacent continental shelf suggest that tidal oscillations in the Strait may be generating the waves.

It is possible to show the origin and decay of a wave by observing the nature of the energy flux along ray paths. For any particular tidal constituent the total energy flux averaged over a tidal cycle is

$$\bar{\mathbf{F}} = \overline{\mathbf{q}p} = \mathbf{q}_p P^0/2, \tag{1a}$$

where $\mathbf{q}$ and p are the instantaneous velocity and pressure which vary sinusoidally in time, P^0 is the maximum pressure and $\mathbf{q}_p$ is the velocity vector at the instant of maximum pressure. Direction of flux is given by the velocity vector at maximum pressure. Proof is presented in the Appendix, and follows the development of Henry and Foreman (1977).

Average energy flux of the shelf and Kelvin waves which comprise the total motion can be written

$$\bar{\mathbf{F}} = V_k^0 P_k^0/2 \quad \text{(Kelvin)} \tag{1b}$$

$$= V_s^0 P_s^0/2 \quad \text{(shelf)}, \tag{1c}$$

where P_k^0 and P_s^0 are the amplitudes of the individual Kelvin and shelf waves. It is assumed here that the waves are neither growing nor decaying and that the topography is uniform alongshore. In such a case alongshore velocities and pressure are in phase (or 180° out of phase) and flux vectors are parallel to shore. The values V_k^0 and V_s^0 here represent peak alongshore velocities of these respective waves. To find the total flux of a wave, (1b) and (1c) must be integrated in the vertical and cross-shelf directions.

If the motion is barotropic, such that η_T^0, η_k^0 and η_s^0 are the respective heights of the total motion, Kelvin and shelf waves respectively, ρ is density and g is gravity, the vertically integrated energy fluxes are

$$\bar{\mathbf{F}}_{\text{int}} = \rho g \mathbf{q}_p \eta_T^0 \frac{H}{2} \quad \text{(total)} \tag{2a}$$

$$= \rho g V_k^0 \eta_k^0 \frac{H}{2} \quad \text{(Kelvin)} \tag{2b}$$

$$= \rho g V_s^0 \eta_s^0 \frac{H}{2} \quad \text{(shelf)}, \tag{2c}$$

where H is the local water depth, assumed to be much greater than the surface displacements.

Over the continental shelf the diurnal-period currents appear to be barotropic; current ellipses are uniform with depth, and only when currents over the slope are examined do any baroclinic effects emerge. Therefore (2a–c) may be applied to currents in shelf waters.

Vertical integrals of the observed current ellipses at K_1 period derived from winter data are presented in Fig. 1. The ellipse in Juan de Fuca Strait is from Godin *et al.* (1980) while G. Cannon and J. Holbrook provided the dimensions for the ellipse near 48°N on the shelf, and H. Freeland the northernmost ellipse from his mooring in 1981. From (2a) it is observed that the lines in these ellipses which represent the vertically integrated current at time of maximum height of the K_1 constituent are proportional to the vertically integrated energy flux. Energy flux is toward the southeast at the southern end of Vancouver Island, and is clearly up-Strait in Juan de Fuca. The line in the ellipse at 47°47′N represents a very small flux toward the northeast. Elsewhere $\bar{F}_{int}$ is in every direction but to the northwest, the direction expected for both Kelvin and first-mode shelf waves.

This spatial distribution of energy flux is examined in Section 2 with the aid of numerical solutions of the geophysical equations. In Section 3 these are compared with observations, and estimates of the alongshore energy flux in the shelf and Kelvin waves are presented to show the nature of the generation and decay of the shelf waves.

2. Energy flux of shelf and Kelvin waves

a. Individual shelf and Kelvin waves

Numerical integration of the linearized, shallow water equations (Henry *et al.*, 1984) produces cross-shelf pressure and velocity distributions for Kelvin waves whose wavelength at K_1 period (23.93 h) is 13 000 km. A solution of the baroclinic equations (kindly provided by K. Brink of Woods Hole Oceanographic Institution, Brink, 1982) gives a first-mode shelf wavelength of 270 km at K_1 period, and a pressure and velocity field that vary cross-shelf and also with depth. The velocities of these two waves were compared by a least-squares fit to the observed currents at 16 or more current meters off Estevan Point (CT84). Amplitude of the shelf wave at shore predicted by the model (5 cm) agrees well with that

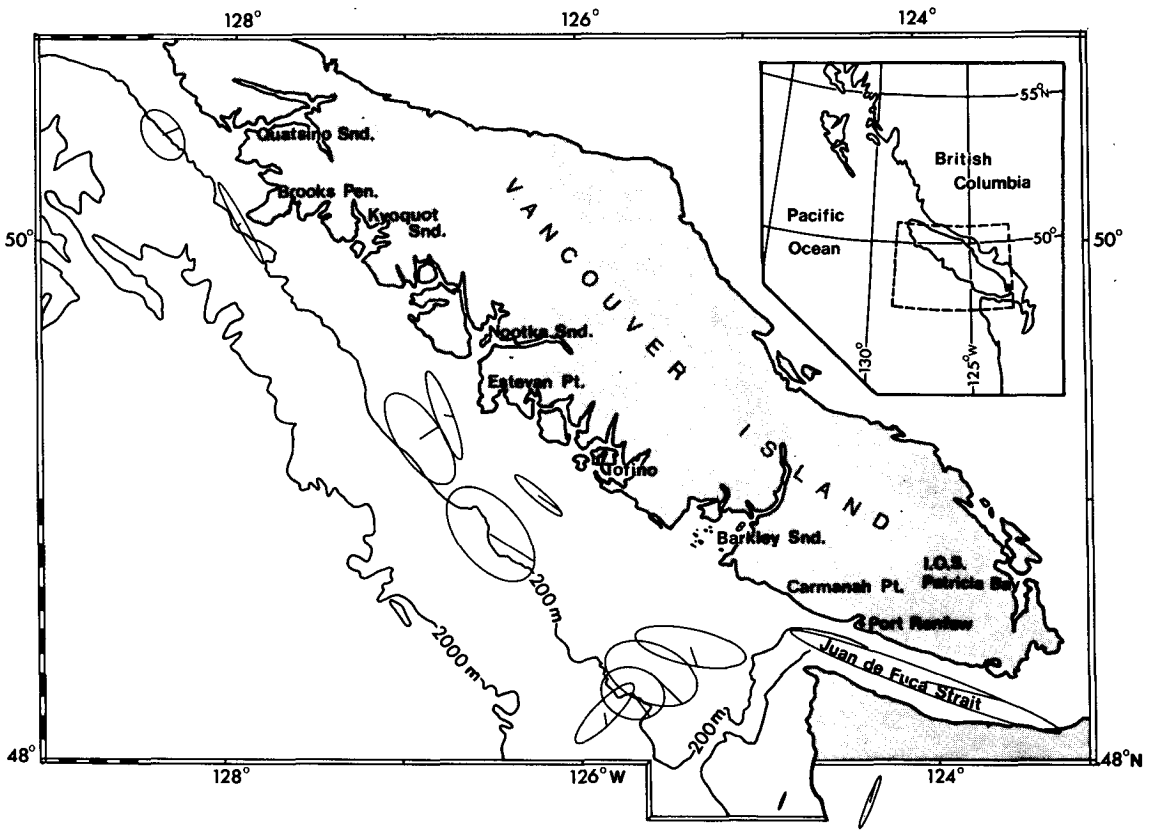

FIG. 1. Ellipses of the vertically integrated K_1 current in winter observed along the Washington and Vancouver Island coastline. Lines in ellipses represent time averages of F_{int}. The southernmost ellipse is replotted at right at three times the size to show the vector $\bar{F}_{int}$.

observed in the pressure records at shore, but the predicted Kelvin-wave height is too small by a factor of 2, on account of the inadequacy of Kelvin-wave theory in this region (CT84). However, the spatial distribution of height and current is predicted well by Kelvin-wave theory within 100 km of shore, and a 43 cm Kelvin wave will be used to model the K_1 surface tide here.

Velocities and pressures given by the numerical solutions for the Kelvin wave are used in (1b) to give a depth-independent energy flux $\bar{\mathbf{F}}$, plotted in Fig. 2a. (Velocity and pressure contours themselves are given by CT84). Because the offshore decay scale of Kelvin waves is the Rossby radius (2000 km), which is much greater than the continental shelf width, its flux magnitude changes little within 150 km of shore. Energy flux is always parallel to shore (no friction and no energy input) for these modeled currents; therefore only the alongshore flux is contoured. Flux is always prograde (in the direction of phase propagation).

Energy flux for a baroclinic shelf wave [Fig. 2b, computed from (1c)] decreases away from shore, changes sign near the outer shelf, and reverses again farther offshore. It is a general rule for shelf waves that the number of these bands is $2n + 1$ where n is the mode number of the wave; here the first mode displays three bands. This banding arises because the sign of the alongshore energy flux depends upon the sign of the product of alongshore velocity times pressure. These two variables have zero-crossings at different distances from shore. Where they have the same sign, the energy flux will be in the direction of phase propagation; where signs differ, the flux will be reversed, or retrograde.

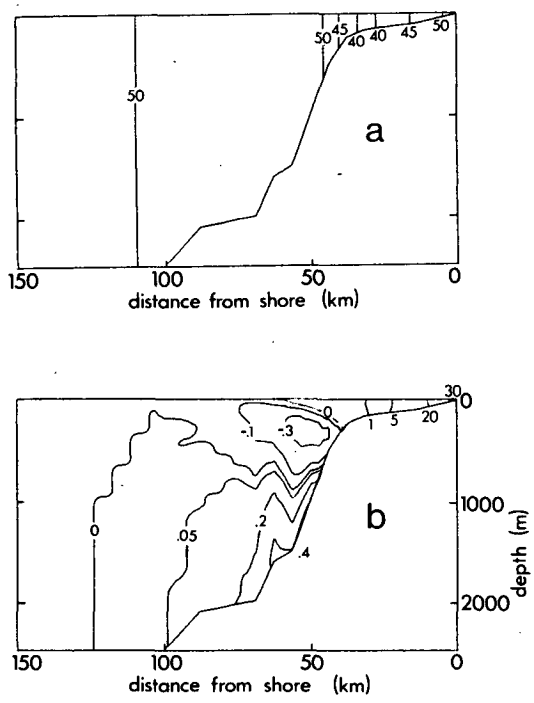

FIG. 2. Contours of energy flux of K_1-period waves along Vancouver Island, at Estevan Point: (a) barotropic Kelvin wave; (b) first-mode baroclinic shelf wave. Units are W m^{-2}.

Retrograde energy flux in the center band can be comparable to, or even larger in magnitude than, the sum of the prograde energy flux in the two outside bands (Davis, 1981), and it can be shown (R. F. Henry, personal communication, 1982) that in a shelf wave of zero group velocity (as determined from where the dispersion curve has a slope of zero) the net energy flux in these three bands is zero. Figure 2b shows the retrograde energy flux in the middle band to be small at Estevan Point, as is confirmed by the dispersion curve for this bottom topography (CT84). At Estevan Point then, the net energy flux is to the northwest in the direction of phase propagation.

b. Superimposed Kelvin and shelf waves

When the K_1 Kelvin wave (λ = 13 000 km) is superimposed upon the baroclinic shelf wave (λ = 270 km), the resulting energy flux assumes a much different pattern. The instantaneous flux is now

$$\mathbf{F} = \mathbf{q}p = (\mathbf{q}_s + \mathbf{q}_k)\cdot(p_s + p_k) \approx (\mathbf{q}_s + \mathbf{q}_k)p_k, \quad (3)$$

where the subscripts s and k refer to the shelf and Kelvin waves respectively. A first-order approximation gives $p_k \gg p_s$, permitting one to drop p_s in (3). Since p_k is depth-independent, the barotropic equation for flux may be used if the vertically averaged current is known, even if the motion is strongly baroclinic.

The individual currents combine to a total current ellipse, $\mathbf{q}_T = \mathbf{q}_s + \mathbf{q}_k$. Instantaneous energy flux becomes

$$\mathbf{F} = \mathbf{q}_T p_k, \quad (4)$$

while the average vertically integrated flux is

$$\overline{\mathbf{F}_{\text{int}}} = \rho g H \mathbf{q}_{Tp} \frac{\eta_k^0}{2}, \quad (5)$$

where H is the water depth and $\mathbf{q}_{Tp}$ the vertically averaged, total current vector at the instant of maximum pressure, which in this case coincides with the time of maximum elevation of the tidal constituent K_1. As before, energy flux direction coincides with the direction of flow at high water of the K_1 constituent.

The overall pattern plotted in Fig. 3 represents the cross-shelf and along-shore distribution of current of these two waves for an idealized bottom topography similar alongshore to that found off Estevan Point, where the depth drops to 2500 m at 100 km from shore.

Flux vectors in the ellipses represent portions of continuous flux lines which cannot be broken, as

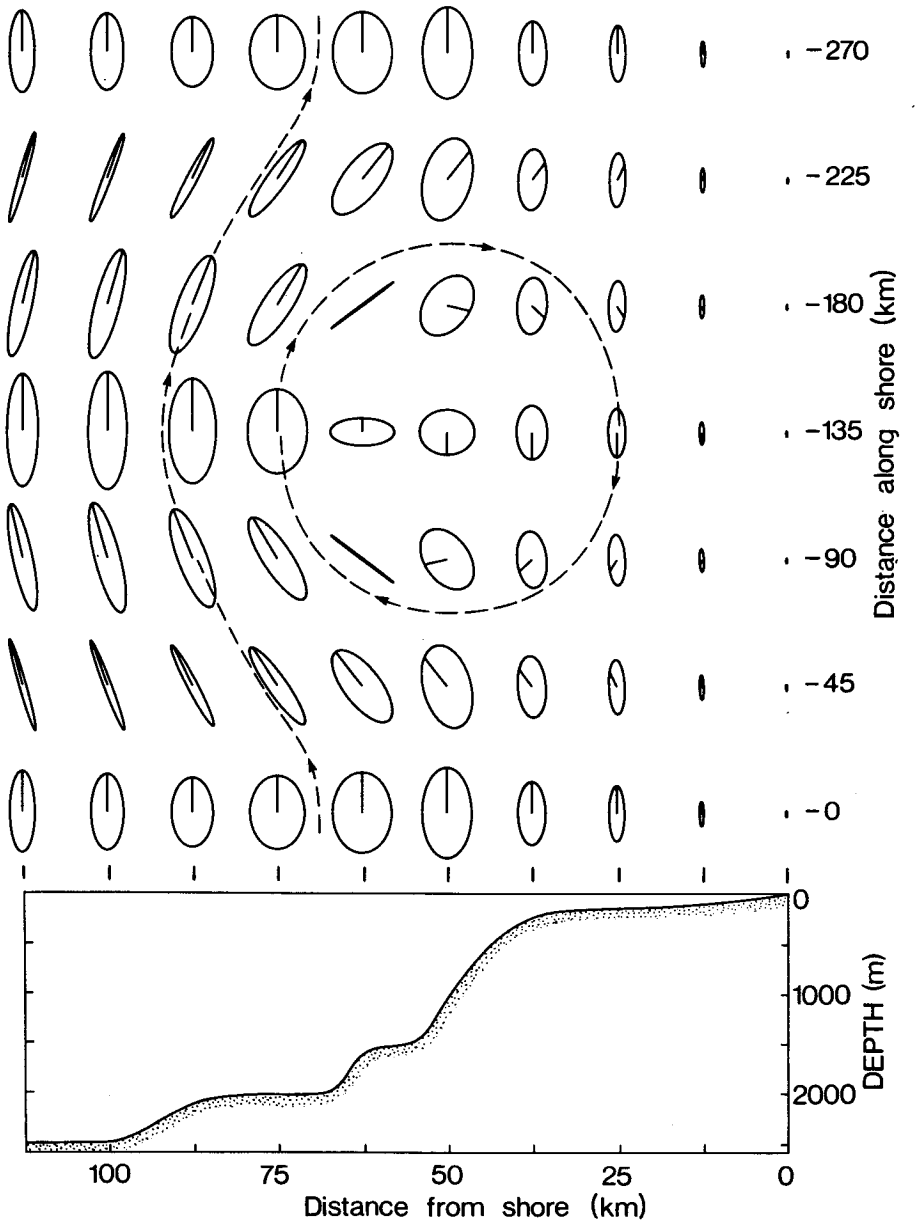

FIG. 3. Ellipses of the vertically integrated current at K_1 period for a coastline whose offshore depth profile is that found off Estevan Point. Pattern represents one wavelength of a baroclinic shelf wave superimposed upon a Kelvin wave of infinite wavelength. Lines in ellipses represent the time average of $\mathbf{F}_{int}$.

these hypothetical waves are nondissipative, with no energy source. Dashed lines in Fig. 3 represent two continuous flux lines. One shows the meander; the other reveals a gyre of flux lines over the shelf.

3. Comparison with observed flux vectors

The results of Section 2 indicate that the energy-flux vectors in Fig. 1 should fit into a pattern of gyres and meanders along Vancouver Island, but these should differ from the ideal case found in Fig. 3 because the continental shelf along Vancouver Island decreases in width toward the north. Off Carmanah Point the shelf break is found at 80 km from shore, while at Brooks Peninsula the shelf extends out only 10 km. Where the shelf is narrower, wavelengths of shelf waves decrease (CT84), forcing shorter gyres over the shelf; the narrow shelf restricts the width of the gyres and the sum of these two changes produces a much smaller gyre at the north end of Vancouver Island.

An attempt to represent the proper pattern of $\bar{F}_{int}$ in Fig. 4 takes these factors into account. It is a freehand diagram, and neglects the effect of dissipation or dispersion in the shelf wave. Gyres were shaped to match the observed directions at the current meter positions and also the shore-based tide gage data given by CT82. Energy flux is directed northward over the continental shelf only between Estevan Point and Brooks Peninsula. Because this portion of the shelf lacks current meters, it is now obvious why none of the flux directions in Fig. 1 points toward the northwest.

Flux lines are not plotted southward from Juan de Fuca Strait, as the behavior of the waves in this region is not well known. Measurements immediately to the south of Juan de Fuca Canyon are not available, but the mooring at 47.47°N, 124.9°W maintained by G. Cannon and J. Holbrook of PMEL (personal communication, 1983) shows a very small flux vector pointed to the northeast. If a shelf wave is present here, it is very weak with currents comparable to those of the Kelvin wave. Observations within Juan de Fuca Canyon (G. Cannon, personal communication, 1983) near bottom reveal an energy flux up canyon toward Juan de Fuca Strait.

Magnitudes of the energy flux can be evaluated in Juan de Fuca Strait, and across the Carmanah, Estevan and Quatsino Lines. A 1973 study of currents in Juan de Fuca Strait (Huggett *et al.*, 1976) provides sufficient data to resolve the current and height of the K_1 tide there. A flux of 1060 ± 150 Megawatts of energy at K_1 frequency up Juan de Fuca Strait is computed from the values of U^0, η^0, ρ, H, width of the Strait and phase difference between peak velocity and height (61°) given by Godin *et al.* (1980) in their analysis of these data. No estimates of errors are given by these authors, but reasonable uncertainties are ±10% for speed U^0, ±3% for height η^0 and lesser values for phase, giving a cumulative uncertainty of 150 Megawatts.

Across the lines which extend offshore from Vancouver Island, observations are too widely separated in space to permit direct computation of the flux; instead the numerical values of the modeled currents are fitted to the observations to calibrate the model Kelvin and shelf waves. Then the product of the pressure and velocity fields of the waves are put into (1b) and (1c) and integrated to give the flux for these waves. Of the shelf wave fluxes, the best estimate lies along the Estevan Line. Four separate values of $\bar{F}_{int}$ across this line derive from four separate mooring deployments of four months each (CT84). Current

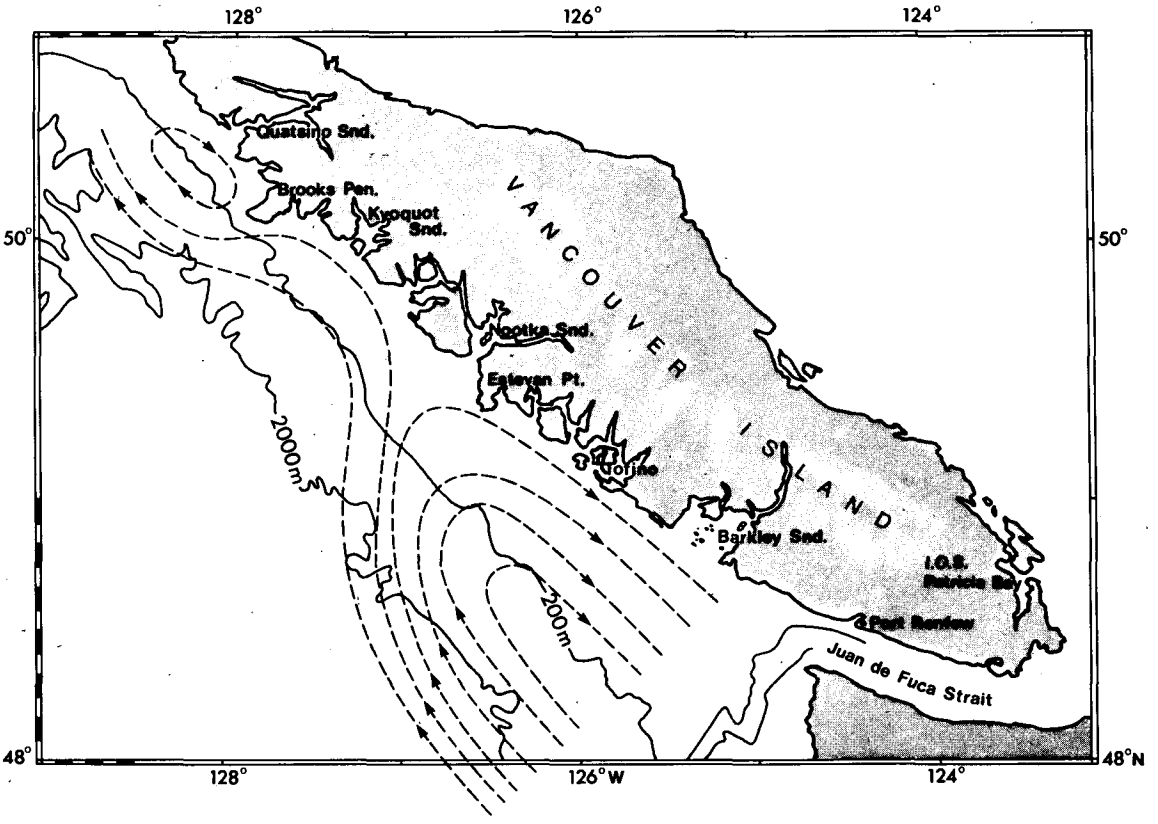

FIG. 4. Expected pattern of K_1 energy flux lines off Vancouver Island fitted to the known flux vectors at current meter moorings.

meters were well distributed over at least five moorings between shore and 100 km offshore, and between 92 and 94% of the variance of these current meters was accounted for by a shelf wave alone (CT84). The four values of $\bar{F}_{int}$ for these deployments are 45, 44, 50 and 48 megawatts, values which are remarkably consistent and suggest an uncertainty of 3 megawatts. Additional errors might be due to the shortcomings of the numerical model of Brink, but the model fits the data so well that I have assigned a value of 4 megawatts to this latter error to match the 8% of variance in the current meter records unexplained by the shelf wave in the worst case noted above. Fitted energy flux is then 47 ± 7 megawatts.

Confidence in $\bar{F}_{int}$ for the shelf wave diminishes at the Quatsino Sound and Carmanah Lines. A fishing bank running parallel to the Carmanah Line near mooring C1 deflects the K_1 current such that the behavior of the flux within 40 km of shore is uncertain by about 30%. Variance of the currents at eight meters on deeper moorings is better fit to the shelf-wave model, with almost 90% accounted for by the shelf wave. It is this fit that gives a value of $\bar{F}_{int}$ of 84 megawatts, but 68 megawatts of the total crosses the Carmanah Line within 40 km of shore, giving an uncertainty of 20 megawatts here alone. If the other factors noted at Estevan Point contribute a proportional uncertainty, then the value of $\bar{F}_{int}$ is 84 ± 32 megawatts.

Only one mooring with three current meters is available at Quatsino Sound, and its location at the 200 m contour places it barely within a region of strong shelf-wave currents. Rather than attempt a least-squares fit with both waves, the appropriate Kelvin-wave currents for a 43 cm high wave were subtracted from the observed K_1 currents. Residual currents at the three depths were fit to the modeled shelf wave currents to give a flux of 8 megawatts. Depth contours in deeper waters along this line are more irregular than along the Estevan Line, and the validity of the cross-shelf distribution of velocities cannot be tested properly. However, even if the uncertainty in the energy flux is comparable to the flux itself, a reasonably high value given the lack of data, energy in the wave here estimated at 8 ± 8 megawatts is considerably less than observed at Estevan Point.

In a similar fashion one derives the Kelvin-wave flux. The distribution of $\bar{F}$ in Fig. 2a indicates that this wave, although shore-trapped, decays very slowly away from shore. To compare with the shelf wave, the Kelvin-wave flux between shore and the 1000 m contour off Estevan Point is computed. A 43 cm high wave carries 500 megawatts across this section. As discussed in Section 2, the observed currents indicate that the Kelvin wave should be only about 22 cm high, about one-half the height of the observed wave. Since the currents of the 43 cm high wave are used for the estimate of 500 megawatts, this value may be high by 50%. The height of 43 cm is accurate to within 2 cm, or 5%. These effects widen the range to 220 to 550 megawatts for the Kelvin wave.

A final calculation of energy flux can be made, one which may be the most interesting. If one combines the shelf-wave currents with the Kelvin-wave pressure field and integrates along the Carmanah Line from shore to the 1000 m contour, then the retrograde energy flux in the shoreward arm of the gyre can be calculated. Shelf-wave currents here are within a few degrees of direct opposition to the Kelvin-wave currents, placing this line almost on the portion of the gyre with maximum energy flux in the direction opposed to the overall flux of the wave, such as observed in row 4 of Fig. 3. The gyre center sits at the point where Kelvin- and shelf-wave currents are equal in magnitude and cancel; here it is at the 1000 m contour. This computed flux is 2200 megawatts, assuming a uniform 43 cm high Kelvin wave. Errors are about 300 megawatts on account of the deflection by the bank, 300 megawatts on account of lack of confidence in the fit, and 200 megawatts on account of variations in height along the line, giving an estimated 2200 ± 800 megawatts. This energy flow must be redirected suddenly near Juan de Fuca canyon, since the suspected flux in waters south of the canyon is small. Much of it must flow up Juan de Fuca Strait where the energy transport rate is 1060 ± 150 megawatts.

All estimates are listed in Table 1. Any value that requires Kelvin-wave currents or heights must be terminated at some distance from shore, as the offshore decay scale of Kelvin waves is too large to be relevant to shelf-wave dynamics. No estimates are given for Tofino data, where current meters were in either the surface or bottom-boundary layers, or at Brooks Peninsula where abrupt alongshore changes in isobaths diminish confidence in the wave models.

4. Discussion and conclusion

The total energy flux due to the shelf wave and Kelvin wave does appear to form the gyres and meanders over the continental margin that the pattern in Fig. 3 reveals. To provide a consistent picture only winter data were presented in Fig. 4 to fit an expected flux pattern to the observations. At the Carmanah Line, shelf-wave phases shift little from summer to winter, but this shift increases along the coastline, reaching 60° in phase at Brooks Peninsula, with longer wavelengths in winter (CT84). Summer wavelengths are sufficiently short that the entire pattern shifts southward, with a larger excursion at Brooks and almost no movement at Carmanah, an effect attributed by CT84 to a cross-shelf shear in average currents. It is interesting to observe that although the total flux vectors are shifted significantly, the magni-

TABLE 1. Energy flux estimates.

Total energy flux	Region	Flux (megawatts)	Method
Total energy flux (Eq. 5)	Juan de Fuca Strait, Pillar Point to Jordan R.	910–1310 up-Strait	Analysis of current meter and tide gage records across Strait, deployed March to June 1973
	Carmanah Line shore to 1000-m isobath	1400–3000 to southeast	Shelf-wave current field is given by model of Brink (1982) fitted to observed currents. Heights are given by (Henry *et al.*, 1984) model Kelvin wave, fitted to 43 cm high wave
Shelf wave (Eq. 1c)	Carmanah Line	52–116 to northwest	Currents are from Brink's (1982) model, fitted to observations. Shelf-wave pressure is specified by model once currents are known
	Estevan Line	40–54 to northwest	Same as Carmanah
	Quatsino Line	0–16 to northwest	Same as Carmanah
Kelvin wave (Eq. 2b)	Estevan Point, shore to 1000-m isobath	220–550	Heights are from Henry *et al.* (1984) model fit to a 43-cm-high Kelvin wave. Currents are specified once heights are known

tude of the flux of the shelf wave is unaffected. Of the four estimates of shelf-wave flux at Estevan Point, summer values of 45 and 48 megawatts do not differ significantly from those of 44 and 50 observed in winter.

There is no evidence that the shelf wave propagates southward. All reported currents in the region south of the entrance to Juan de Fuca are close in magnitude to the Kelvin-wave currents alone (Cannon, personal communication, 1983; Torgrimson and Hickey, 1979). These observations agree with theoretical considerations (CT84), based upon recent work of Chapman (1983).

It is most likely then that the shelf wave originates at the entrance to Juan de Fuca Strait and is prevented from southward propagation by the absence of any known waves able to carry energy southward. From the available flux estimates the wave loses most of its energy rapidly, decaying by about 90% at Quatsino which is about one wavelength downstream. The model of Brink (1982) provides a frictional decay distance for long-wavelength shelf waves. For the K_1 wave at Estevan Point this distance is 3000 km, or 10 times the distance from Carmanah to Quatsino. Therefore the observed decay of the waves is more likely to be due to wave dispersion than to frictional effects.

The relative phase of the shelf and Kelvin waves observed at Carmanah is the only superposition that will permit these two individual waves to carry energy to the southeast into Juan de Fuca Strait, and still individually transport energy to the northwest as is required for both of these shore-trapped waves. Future work with numerical models capable of representing the bottom topography at the entrance to Juan de Fuca Strait may reveal the flow of energy in this complicated region and show the relative contributions of Juan de Fuca Strait, the canyon and the bend in the shoreline to the generation of shelf waves here. A model of barotropic K_1 waves in this region (R. Flather, personal communication, 1983) shows the shelf wave to disappear if Juan de Fuca Strait is blocked off in the model. The combined evidence clearly points to Juan de Fuca Strait as a generation region. Future work with numerical models may determine the strength and phase of shelf waves to be found at entrances to other tidal channels where diurnal-period currents and tidal heights are large.

Acknowledgements. I am grateful for the data along the Carmanah Line and at Quatsino Sound provided by H. Freeland, and within the Juan de Fuca Canyon and along the coast of Washington provided by G. Cannon and J. Holbrook. Many of the ideas were developed through conversations with A. F. Bennett and R. F. Henry. K. Brink, D. Chapman, H. Freeland and P. LeBlond, providing valuable criticism, and I am grateful for the baroclinic shelf-wave model provided by K. Brink. Computations and computer graphics are by K. Lee. Manuscript was typed by S. Michaux.

APPENDIX

Tidal Ellipse Equations

The energy equation for frictionless and unforced fluid motion can be written:

$$\frac{D}{Dt}\left(\frac{\rho q^2}{2} - \rho \mathbf{g}\cdot\mathbf{x}\right) + \nabla\cdot(\mathbf{q}p) = 0 \qquad \text{(A1)}$$

(LeBlond and Mysak, 1978), where $\mathbf{x}$ is the position vector of a fluid element, $\mathbf{q}$ the velocity of this element, q^2 the square of the speed, p the pressure and ρ the density. When this equation is integrated over a fixed volume V of a fluid, the resulting equation:

$$\frac{\partial}{\partial t}\iiint_V \left(\frac{\rho q^2}{2} - \rho \mathbf{g}\cdot\mathbf{x}\right)dv = -\iint_S p\mathbf{q}\cdot\hat{\eta}\,dA \qquad \text{(A2)}$$

states that the rate of change of energy within a volume V is the negative of the rate of flux of energy out through the surface S bounding the volume V. The energy flux is then written as $\mathbf{q}p$.

Tidal currents of a single tidal constituent are normally represented by ellipses, with the tip of the instantaneous current vector tracing out the ellipse over a tidal cycle whose period is $T = 2\pi/\omega$.

If θ represents the lag of maximum current behind maximum tidal potential when time $t = 0$ and the x-direction is oriented along the positive semimajor axis, the x- and y-components of the total current $\mathbf{q}$ are

$$u = U^0\cos(\omega t - \theta), \qquad \text{(A3a)}$$

$$v = V^0\sin(\omega t - \theta), \qquad \text{(A3b)}$$

Pressure changes due to the tide can be represented by

$$p = P^0\cos(\omega t - \theta_\eta), \qquad \text{(A3c)}$$

where θ_η is the phase lag of maximum pressure behind maximum tidal potential.

Instantaneous energy flux $\mathbf{q}p$ of the constituent K_1 can be integrated over a tidal cycle to give the average flux in the x and y directions

$$x: \quad \frac{U^0P^0}{2\pi}\int_0^T \cos(\omega t - \theta)\cos(\omega t - \theta\eta)dt = \frac{U^0P^0}{2}\cos(\theta_\eta - \theta), \qquad \text{(A4a)}$$

$$y: \quad \frac{V^0P^0}{2\pi}\int_0^T \sin(\omega t - \theta)\cos(\omega t - \theta\eta)dt = \frac{V^0P^0}{2}\sin(\theta\eta - \theta). \qquad \text{(A4b)}$$

The resultant energy flux vector has horizontal components

$$\bar{\mathbf{F}} = \frac{P^0}{2}[U^0\cos(\theta - \theta\eta)\mathbf{i},\ V^0\sin(\theta - \theta\eta)\mathbf{j}]. \qquad \text{(A5)}$$

At time of maximum pressure of the K_1 constituent, ωt must equal $\theta\eta$ for (A3c) to reduce to $p = P^0$. At this time the current vector is given by

$$\bar{\mathbf{q}}_p = [U^0\cos(\theta - \theta\eta)\mathbf{i},\quad V^0\sin(\theta - \theta\eta)\mathbf{j}]$$

which is in the direction of average energy flux $\bar{\mathbf{F}}$. Therefore the current at high water points in the direction of average energy flux. The average energy flux is now

$$\bar{\mathbf{F}} = \mathbf{q}_p\frac{P^0}{2}. \qquad \text{(A6)}$$

The pressure distribution in a *barotropic* shallow water wave in a homogeneous fluid of density ρ is

$$p = \rho g[\eta^0\cos(\omega t - \theta\eta) - Z], \qquad \text{(A7)}$$

where η^0 is the wave height and Z is the depth of the fluid element below the average water depth. The time average of the energy flux becomes depth-independent, taking the form:

$$\bar{\mathbf{F}} = \rho g\mathbf{q}_p\frac{\eta^0}{2}, \qquad \text{(A8)}$$

and the vertically integrated flux is

$$\bar{\mathbf{F}}_{\text{int}} = \rho g\mathbf{q}_p\eta^0\frac{H}{2}. \qquad \text{(A9)}$$

REFERENCES

Brink, K. H., 1982: A comparison of long coastal trapped wave theory with observations off Peru. *J. Phys. Oceanogr.*, **12**, 897–913.

Chapman, D. C., 1983: On the influence of stratification and continental shelf and slope topography on the dispersion of subinertial coastally-trapped waves. *J. Phys. Oceanogr.*, **13**, 1641–1652.

Crawford, W. R., and R. E. Thomson, 1982: Continental shelf waves of diurnal period along Vancouver Island. *J. Geophys. Res.*, **87**, 9516–9522.

——, and ——, 1984: Diurnal period continental shelf waves along Vancouver Island: A comparison of observations and theoretical models. *J. Phys. Oceanogr.*, **14**, 1629–1646.

Davis, A. M. J., 1981: The scattering by a headland of the dominant continental shelf wave. *Phil. Trans. Roy. Soc. London*, **A303**, 383–431.

Godin, G., J. Candela and R. de la Paz-Vela, 1980: A scrutiny of the current data collected in a section of the Strait of Juan de Fuca in 1973. Informe tecnico Oc.8001, Centro de Investigacion Cientifica y de Educacion Superior de Ensenada, B.C. Mexico.

Henry, R. F., and M. G. G. Foreman, 1977: Numerical model studies of semidiurnal tides in the southern Beaufort Sea. Pacific Mar. Sci. Rep. 77-11. Institute of Ocean Sciences, Sidney, B.C., 71 pp.

——, W. R. Crawford and R. E. Thomson, 1984: Calculation of dispersion curves and modal shapes of continental shelf waves (in preparation).

Huggett, W. S., J. S. Bath and A. Douglas, 1976: Data record of current observations, Vol. XV. *Juan de Fuca Strait 1973.* Institute of Ocean Sciences, Sidney, B.C. Canada.

LeBlond, P. H., and L. A. Mysak, 1978: *Waves in the Ocean. Oceanography Series*, Vol. 20, Elsevier, 602 pp.

Thomson, R. E., and W. R. Crawford, 1982: The generation of diurnal period shelf waves by tidal currents. *J. Phys. Oceanogr.*, **12**, 635–643.

Torgrimson, G. M. and B. M. Hickey, 1979: Barotropic and baroclinic tides over the continental slope and shelf off Oregon. *J. Phys. Oceanogr.*, **9**, 945–961.